NM WRRI Student Water Research Grant Final Report

**1. Student Researcher:** Tarek Ahasan (Department of Civil Engineering, NMSU)

**Faculty Advisor:** Dr. Huiyao Wang (Department of Civil Engineering, NMSU)

**2. Project title:** Innovative Photocatalysts: Revolutionizing Clean Hydrogen Production through Alternative Water and Sunlight Photocatalytic Water Splitting.

## 3. Research objective:

The world is currently grappling with two interconnected challenges: meeting the increasing demand for energy while simultaneously striving to reduce greenhouse gas emissions and enhance energy efficiency [1,2]. The World Energy Outlook 2020 has established a goal of achieving net-zero emissions by 2050, necessitating sustainable development based on clean energy sources and the implementation of specific measures within the next decade to advance toward the target [3]. In response to the concerns over the emission of carbon and assurance of energy supply, the development of green hydrogen technology presents a promising solution for achieving a carbon-neutral future, as green hydrogen serves as a carbon free clean energy source that can help bring the world to a net-zero emissions target [4]. However, finding an efficient and easy process to produce hydrogen gas has become a big challenge today.

The objective of our research project is to synthesize innovative $TiO_2$ based photocatalysts and use the synthesized photocatalysts to produce benign hydrogen energy by utilizing different light sources. To reduce the demand of ultrapure water for water splitting, this study will use different types of alternative water such as tap water, seawater, and produced water as a raw material to produce hydrogen gas. Moreover, the study will examine the treatment of dye wastewater and the simultaneous production of hydrogen from the water.

## 4. Description of methodology employed.

***Step 1. Synthesis of Photocatalysts:***

**Silver-Graphene-Titanium dioxide (Ag-G-$TiO_2$) photocatalyst:** Graphene oxide and $TiO_2$ were dispersed in Deionized water (DI) water and ethanol. Sonication was done to make the solution homogeneous. Then the solution was heated using Teflon-lined stainless-steel autoclave system.

DI water washing and centrifugation was done for the removal of the impurities. The solution was then transferred to the oven for drying. Finally, silver nitrate and sodium citrate dihydrate were added to the dried sample. After that the microwave irradiation was done and the solution was then dried again to obtain the final product.

***Step 2. Characterization:*** Energy-dispersive X-ray spectroscopy (EDS), Transmission Electron Microscopy (TEM), X-ray Diffraction (XRD), Bandgap analyses were done to characterize the synthesized catalyst.

***Step 3. Production of Hydrogen Gas:*** The photocatalytic water splitting was carried out in a closed gas circulation system with external irradiation of quartz reactor. High Pressure UV mercury vapor lamps (160 W PUV-10, Zoo Med Laboratories, CA, US) were used for UV Light Source. In the experiment, ultrapure water, DI water, tap water, different percentages of saline water, synthetic seawater, and produced water were used as a feedstock to produce hydrogen gas. The produced hydrogen gas will be measured using Gas Chromatography.

***Step 4. Analysis of Produced Hydrogen:*** The gas produced during the reaction was measured using an Agilent 7890A gas chromatograph (GC) equipped with a thermal conductivity detector (TCD) and an HP-5 molecular sieve column, with nitrogen ($N_2$) serving as the carrier gas. Calibration of the instrument was performed using a verified sample of pure $H_2$. Subsequently, 1 mL of headspace gas was injected directly into the GC inlet. A purge time of 1 minute was chosen, followed by collection of chromatographic data for 10 minutes post-injection. The standard sample peak retention time (appearance time) and area were compared to the standard $H_2$ sample to calculate the gas concentration.

## 5. Description of results; include findings, conclusions, and recommendations for further research.

### 5.1. Synthesis of Photocatalyst:

*5.1.1. Synthesis of 1 mM Silver-Graphene-Titanium dioxide (1-Ag-G-$TiO_2$) photocatalyst:*

5 ml (5 mg/ml) graphene oxide and 0.5 g of $TiO_2$ were dispersed in 60 ml Deionized water (DI) water and 30 ml ethanol. Sonication was done to make the solution homogeneous. Then the solution was heated for 24 hours at 120 °C using Teflon-lined stainless-steel autoclave system. DI water washing and centrifugation was done for the removal of the impurities from the solution.

The solution was then transferred to the oven for drying at 60 °C. Finally, 30 ml of 1 mM silver nitrate (0.085 g silver nitrate in 500 ml DI water) and 30 ml of 1 mM sodium citrate dihydrate (0.147 g sodium citrate dihydrate in 500 ml DI water) were added to the dried sample. After that the microwave irradiation was done for 3 minutes and the solution was then dried again for 24 hours at 60 °C to obtain the final product.

*5.1.2. Synthesis of 2 mM Silver-Graphene-Titanium dioxide (2-Ag-G-$TiO_2$) photocatalyst:*

The synthesis process remained unchanged apart from the addition of 2 mM silver nitrate (0.170 g of silver nitrate in 500 ml of deionized water) and 2 mM sodium citrate dihydrate (0.294 g of sodium citrate dihydrate in 500 ml of deionized water) to the dried sample, instead of the previous addition of 1 mM silver nitrate and 1 mM sodium citrate dihydrate.

*5.1.3. Synthesis of 4 mM Silver-Graphene-Titanium dioxide (4-Ag-G-$TiO_2$) photocatalyst:*

To synthesize this photocatalyst, 4 mM of silver nitrate (0.338 g of silver nitrate in 500 ml of deionized water) and 4 mM of sodium citrate dihydrate (0.588 g of sodium citrate dihydrate in 500 ml of deionized water) were introduced to the dried sample. The remaining steps of the synthesis process remained unchanged.

*5.1.4. Synthesis of 0.5 mM Silver-Graphene-Titanium dioxide (0.5-Ag-G-$TiO_2$) photocatalyst:*

To produce the catalyst, 0.5 mM of silver nitrate (0.043 g of silver nitrate in 500 ml of deionized water) and 0.5 mM of sodium citrate dihydrate (0.074 g of sodium citrate dihydrate in 500 ml of deionized water) were added to the dried sample. The subsequent steps of the synthesis process remained unaltered.

*5.1.5. Synthesis of Graphene-Titanium dioxide (G-$TiO_2$) photocatalyst:*

For this photocatalyst, only 5 ml of graphene (5 mg/ml) and 0.5 g of titanium dioxide were utilized. No silver nitrate or sodium citrate dihydrate were included in this experiment. However, the synthesis steps remained unchanged.

**5.2. Evaluation of Photodegradation Potential:**

Photocatalytic activity of synthesized G-$TiO_2$, 0.5-Ag-G-$TiO_2$, 1-Ag-G-$TiO_2$, 2-Ag-G-$TiO_2$, and 4-Ag-G-$TiO_2$ was examined using $TiO_2$ as a benchmark to evaluate their performance to degrade

Rhodamine B solution under the visible light irradiation. The wavelength used in the UV spectroscopy analysis was 554 nm.

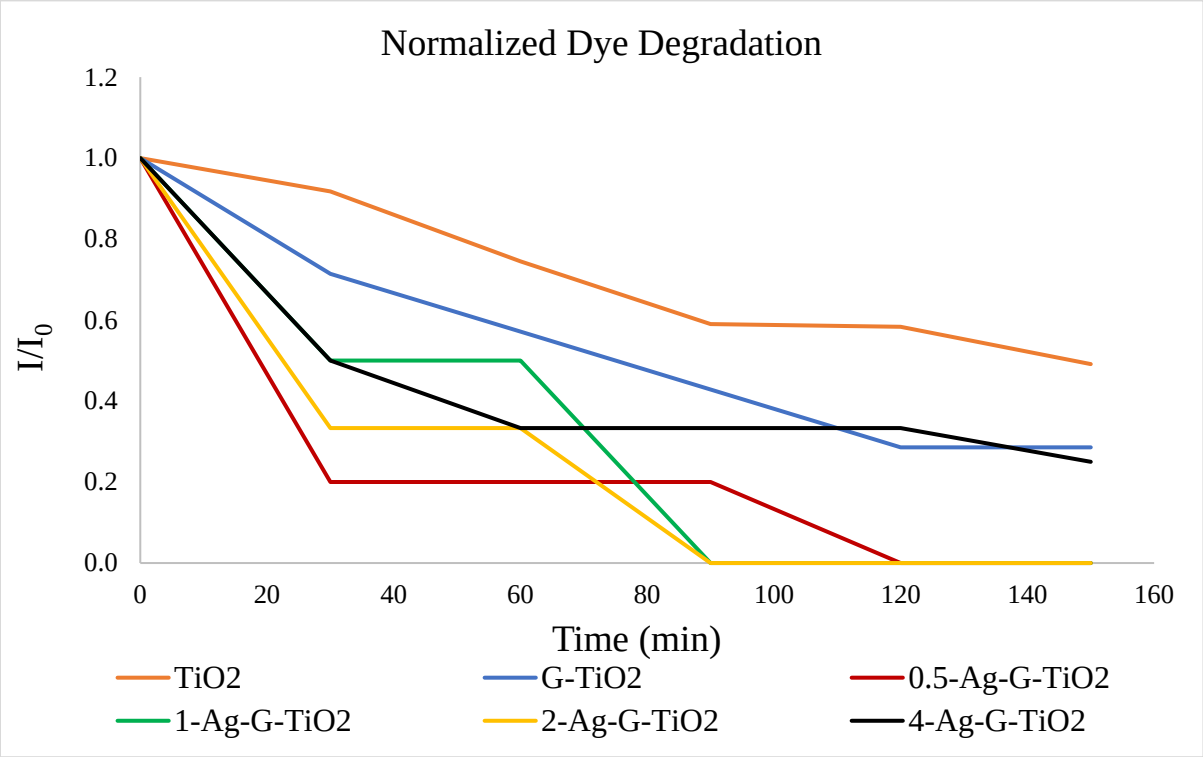


Figure 1: Normalized ($I/I_0$) Rhodamine B dye degradation graph.

From the Rhodamine B dye degradation test (Figure 1), utilizing $TiO_2$, G-$TiO_2$, and 4-Ag-G-$TiO_2$, revealed that the dye concentration did not reach zero within the 150-minute experimental timeframe. Notably, the degradation of dye was least effective when employing only $TiO_2$. Conversely, when using G-$TiO_2$ and 4-Ag-G-$TiO_2$, the final dye concentrations were nearly identical after 150 minutes.

In contrast, the utilization of 0.5-Ag-G-$TiO_2$, 1-Ag-G-$TiO_2$, and 2-Ag-G-$TiO_2$ photocatalysts led to the complete reduction of dye concentration, albeit at varying durations. Specifically, with 0.5-Ag-G-$TiO_2$, the dye concentration reached zero at 120 minutes, while with 1-Ag-G-$TiO_2$ and 2-Ag-G-$TiO_2$, it reached zero at 90 minutes. Notably, during the initial 60 minutes of the experiment, the dye concentration was observed to be higher with 1-Ag-G-$TiO_2$ and lower with 2-Ag-G-$TiO_2$.

Given the superior photodegradation performance exhibited by the photocatalysts, 2-Ag-G-$TiO_2$ has been identified as the optimal choice for conducting water splitting experiments.

## 5.3. Characterization of the synthesized catalyst:

*5.3.1. TEM analysis:*

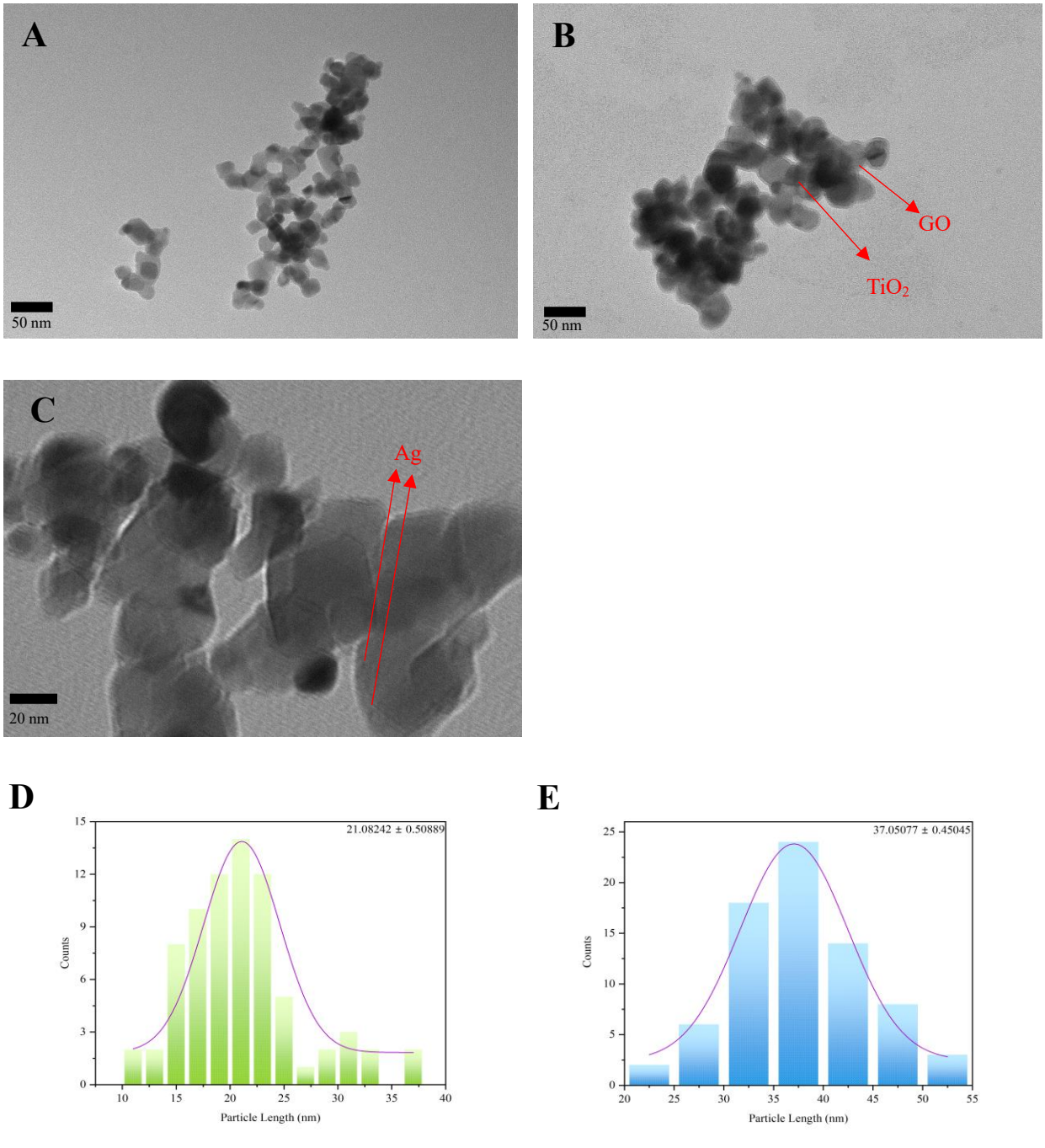


Figure 2: TEM images of the catalysts and their particle size distribution: A) Pure $TiO_2$, B) Ag-G-$TiO_2$, C) 200K magnification of Ag-G-$TiO_2$, D) Pure $TiO_2$, E) Ag-G-$TiO_2$.

TEM analysis revealed distinct morphological differences between pure $TiO_2$ and Ag-G-$TiO_2$ samples. While pure $TiO_2$ particles appeared well-dispersed, Ag-G-$TiO_2$ exhibited an aggregated structure, likely resulting from the deposition of graphene oxide and silver on $TiO_2$ particles. Particle size distribution analysis corroborated these observations, demonstrating that pure $TiO_2$ particles had a smaller average size of 21.08 nm, compared to the larger Ag-G-$TiO_2$ composite particles, which averaged 37.05 nm. This size increase is attributed to the successful incorporation of graphene oxide and silver onto the $TiO_2$ substrate. Examination of Figure 2(B) revealed larger, nearly transparent structures consistent with the presence of graphene oxide, as previously reported [5]. From Figure 2(C), the distributed dark spots observed in the Ag-G-$TiO_2$ were identified as silver nanoparticles [6], indicating successful deposition of Ag. EDS analysis provided further confirmation of the presence of silver particles in the composite.

*5.3.2. EDS analysis:*

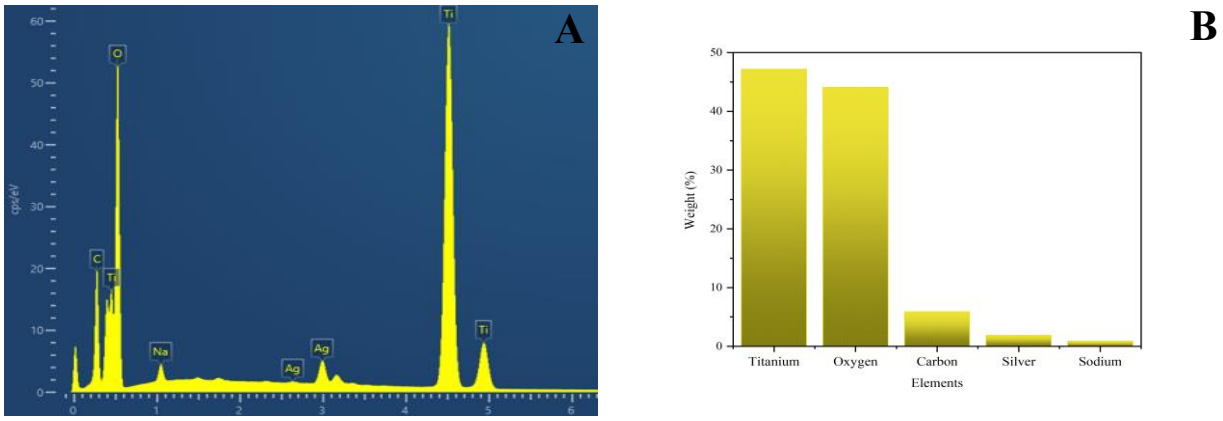


Figure 3: A) EDS analysis of Ag-G-$TiO_2$, B) Weight percentage bar chart of the elements.

EDS analysis provided quantitative elemental composition of the Ag-G-$TiO_2$ composite. Titanium constituted the highest weight percentage at 47.2%, primarily from $TiO_2$. Oxygen, originating from $TiO_2$, graphene oxide, $AgNO_3$, and sodium citrate dihydrate, represented 44.1% of the total weight. Carbon, derived from graphene oxide and sodium citrate dihydrate, accounted for 5.9% of the composite mass. Silver comprised 1.9% of the total weight, corroborating the TEM observations of Ag deposition on $TiO_2$ particles. A minor sodium content (0.9%) was attributed to the sodium citrate dihydrate used in the synthesis process. These results, in conjunction with the TEM analysis, confirm the successful deposition of Ag on the $TiO_2$ substrate.

*5.3.3. Bandgap analysis:*

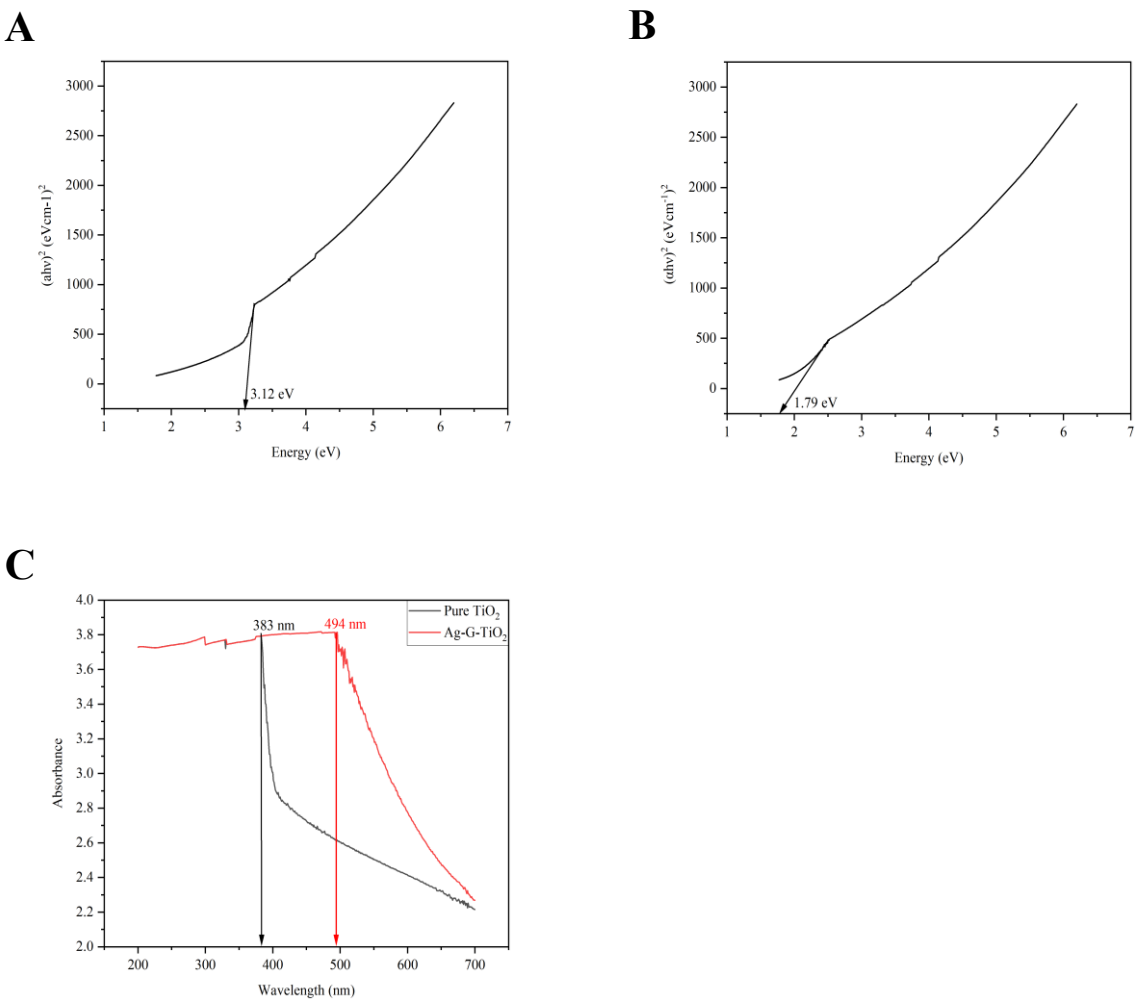


Figure 4: Bandgap analysis for the catalysts A) Pure $TiO_2$, B) Ag-G-$TiO_2$ C) Absorbance comparison between pure $TiO_2$ and Ag-G-$TiO_2$.

UV-vis spectroscopy revealed that the absorption edge for $TiO_2$ occurred at 385 nm, while for Ag-G-$TiO_2$, it redshifted to 494 nm. This redshift indicates the presence of electron acceptors, likely due to the surface plasmon absorption of $Ag^0$. The observed absorption phenomenon can be attributed to charge transfer from the valence band to the conduction band, specifically the transition of electrons from 2p orbitals of oxide anions to 3d orbitals of $Ti^{4+}$ cations [7]. Bandgap calculations showed a significant reduction from 3.12 eV for pure $TiO_2$ (Figure 4(A) to 1.79 eV for Ag-G-$TiO_2$ (Figure 4(B). This narrowing of the bandgap in the nanocomposite facilitates effective assimilation of photoinduced electrons, resulting in the formation of a closed Fermi level

energy between the valence and conduction bands. The consequent decrease in Fermi energy promotes the migration and separation of photoinduced electron-hole pairs, potentially enhancing the photocatalytic performance of the catalyst [8].

*5.3.4. XRD analysis:*

X-ray diffraction analysis was employed to determine the crystal phase and crystallite size of both unmodified $TiO_2$ and Ag-G-$TiO_2$ (Figure 5). Both samples exhibited characteristic peaks corresponding to anatase (JCPDS 78-2486) and rutile (JCPDS 21-1276) phases [9]. Notably, diffraction peaks attributable to Ag were not observed in the Ag-G-$TiO_2$ sample, likely due to its low concentration [10]. Typically, XRD peaks associated with Ag appear at 38.1° and 64.5° when the Ag doping exceeds 2 wt% [11]. A slight shift in the primary $TiO_2$ peak from 25.10° to 24.93° was observed, suggesting the incorporation of $Ag^+$ ions into the $Ti^{4+}$ lattice [12]. The rutile phase content was calculated using the following equation:

$$\text{Rutile phase content (\%)} = A_R / (0.884 \times (A_A + A_R)) \quad \text{---------- (9)}$$

Where $A_A$ and $A_R$ represent the integrated intensities of the diffraction peaks from the (101) and (110) planes of the anatase and rutile phases, respectively. Upon Ag-doping, a slight decrease in the anatase phase of $TiO_2$ was observed, as shown in Table 1. This finding aligns with previous reports in the literature [13].

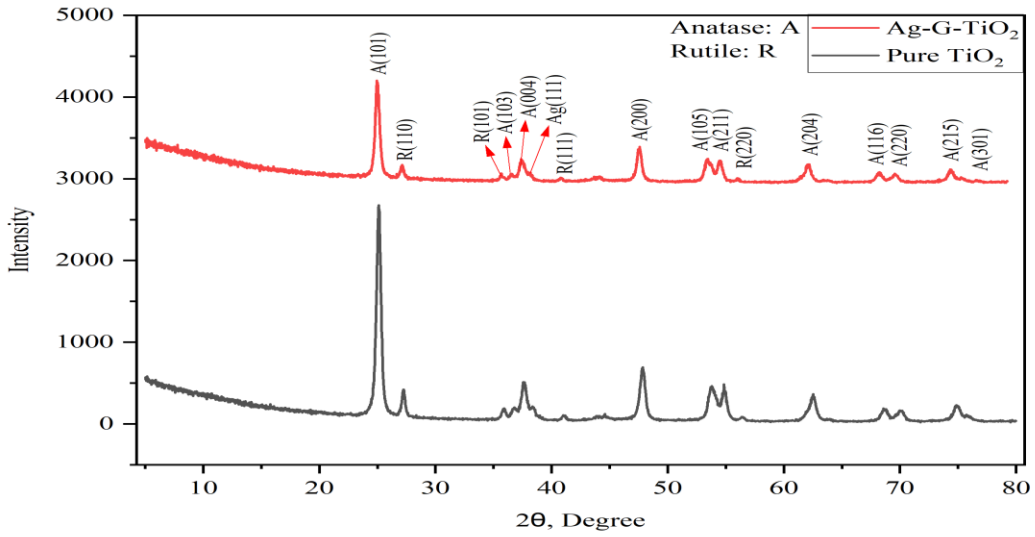


Figure 5: XRD patterns of the pure $TiO_2$ and Ag-G-$TiO_2$.

Table 1: Crystalline phases composition of the photocatalysts.

| Photocatalysts | Crystalline Phase, % | |
|---|---|---|
| | Anatase | Rutile |
| $TiO_2$ | 89.23 | 10.77 |
| Ag-G-$TiO_2$ | 88.89 | 11.11 |

*5.3.5. XPS analysis:*

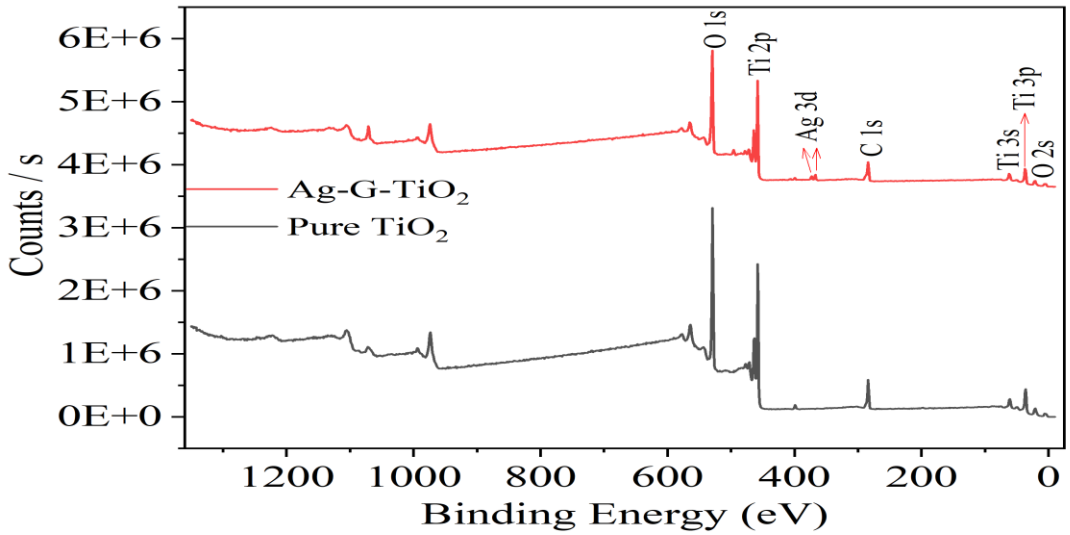


Figure 6: XPS Spectra of pure $TiO_2$ and Ag-G-$TiO_2$.

X-ray photoelectron spectroscopy (XPS) analysis revealed several key insights into the surface chemistry of the materials. The C 1s peak at 283-288 eV was attributed to oxygenated carbon species, likely indicative of graphene oxide incorporation [14]. The peak at ~288 eV suggested the presence of C-O bonds, implying that carbon may have substituted for some lattice titanium atoms, forming a Ti-O-C structure [15]. The carbon content was determined to be 2.43 wt.%. The Ag 3d peak at ~367 eV indicated potential electronic interactions between the metal and support, via charge transfer at the metal-support interface, forming a Ti-Ag-O phase [16]. The silver content was 1.98 wt.% based on the XPS analysis. The weight percentages of Ag determined by the XPS analysis was corroborated by the result from EDS measurement. The High-resolution Ti 2p spectra

(Figure 7A) showed a higher proportion of $Ti^{3+}$ (60.34%) at 458.32 eV compared to $Ti^{4+}$ (30.30%) at 464 eV, suggesting the removal of oxygen from the $TiO_2$ lattice. Ag doping appeared to increase the $Ti^{3+}$ content while decreasing $Ti^{4+}$, potentially indicating the formation of $Ti_2O_3$ or mixed Ag-$Ti^{3+}$ oxide structures [17]. The O 1s spectra displayed two peaks at 529.54 eV and 531.36 eV (Figure 7B), corresponding to Ti-O bonds and oxygen vacancies, respectively. The high density of oxygen vacancies is expected to enhance charge transfer at the interface, improving the overall photocatalytic performance [18]. The peaks at 38 eV and 61 eV is because of the Ti 3p and Ti 3s, respectively [19].

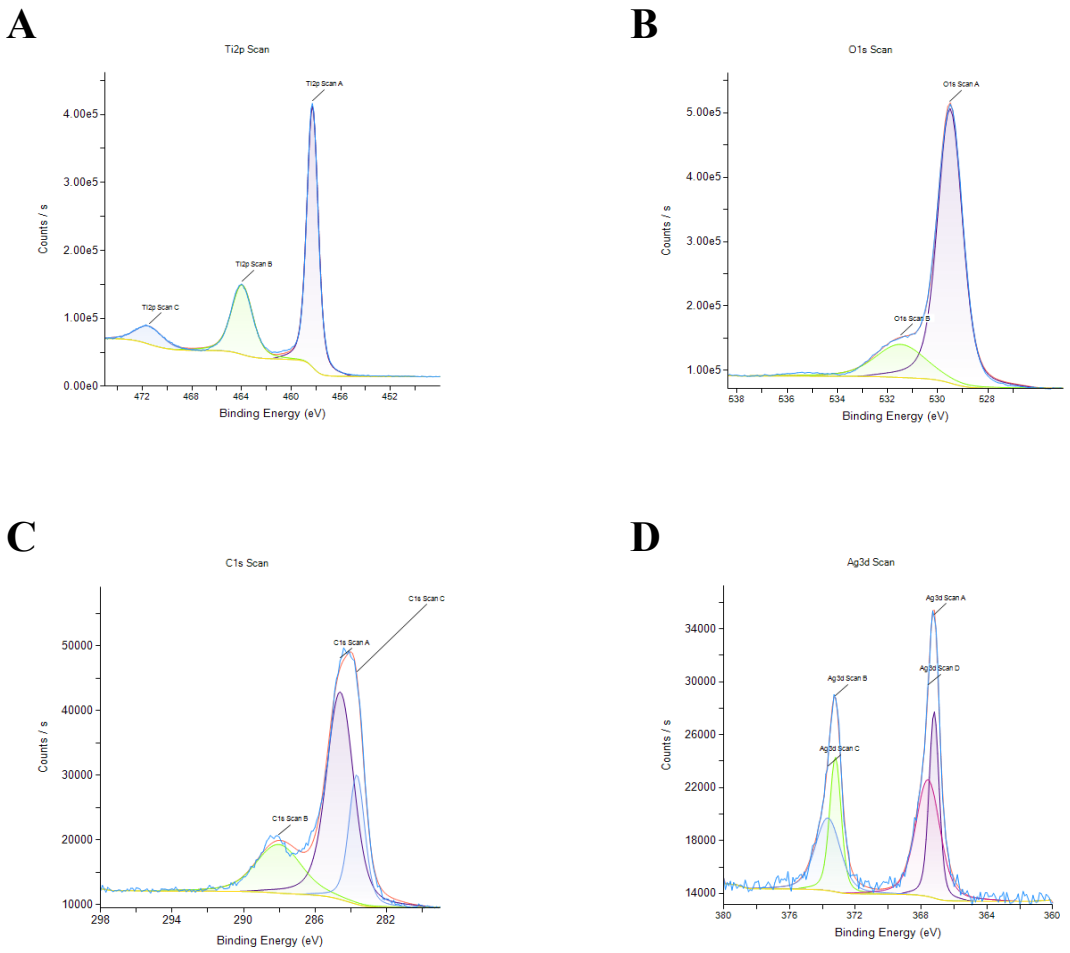

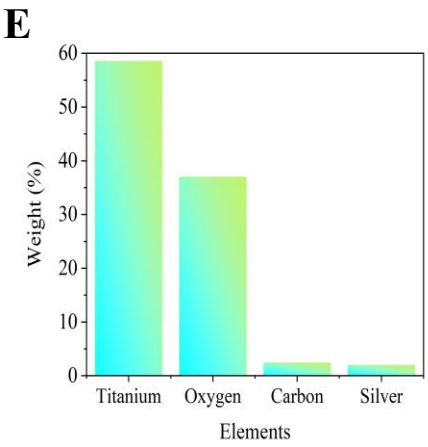


Figure 7. XPS Spectra of A) Ti 2p, B) O 1s, C) C 1s, D) Ag 3d, E) Elemental weight per-centage.

*5.3.6. Nitrogen adsorption-desorption analysis:*

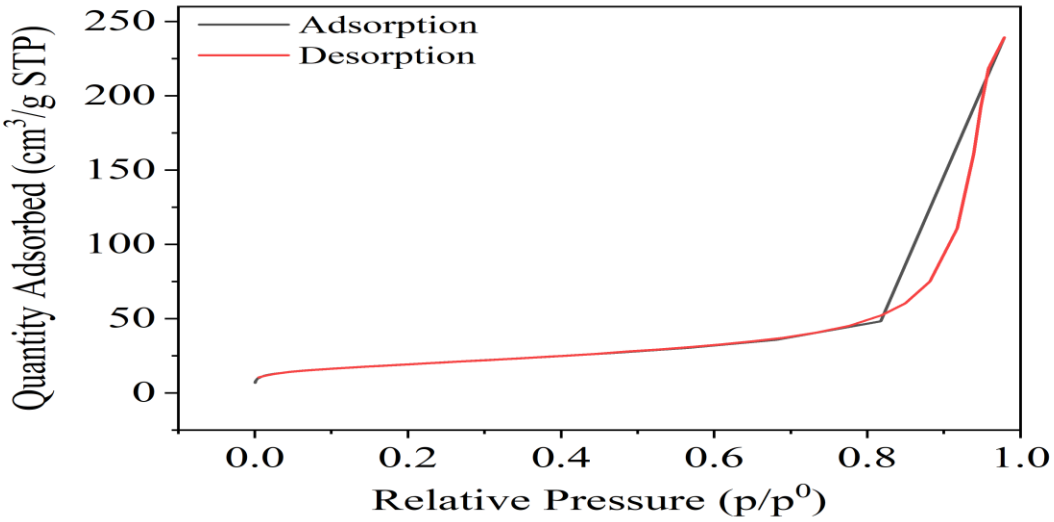


Figure 8. Adsorption isotherm of Ag-G-$TiO_2$ catalyst.

The nitrogen adsorption-desorption isotherm for the synthesized catalyst exhibited a Type IV profile (Figure 8). Initially, the nitrogen uptake was low, but increased rapidly when the relative pressure exceeded 0.8. This isotherm shape is characteristic of mesoporous materials. The Brunauer-Emmett-Teller (BET) surface area of the synthesized catalyst was determined to be 69.00 m2/g, which is significantly higher than the 37.56 $m^2$/g surface area of pure $TiO_2$ [20]. This enhancement is likely attributed to the incorporation of graphene oxide into the catalyst structure [21]. Analysis of the pore size distribution revealed an average Barrett-Joyner-Halenda (BJH)

adsorption pore diameter of 55.019 Å and an average BJH desorption pore diameter of 225.6 Å, indicating that the catalyst contained predominantly mesoporous features (Table 2). The Langmuir surface area of the catalyst was determined to be 45.67 $m^2/g$.

Table 2. Surface area and porosity of the synthesized catalyst.

| | |
|---|---|
| BET surface area | 69.00 $m^2/g$ |
| Langmuir surface area | 45.67 $m^2/g$ |
| BJH adsorption cumulative pore volume | 0.065 $cm^3/g$ |
| BJH desorption cumulative pore volume | 0.388 $cm^3/g$ |
| BJH adsorption average pore diameter | 55.02 Å |
| BJH desorption average pore diameter | 225.58 Å |

## 5.4. Photocatalytic Water Splitting Experiment:

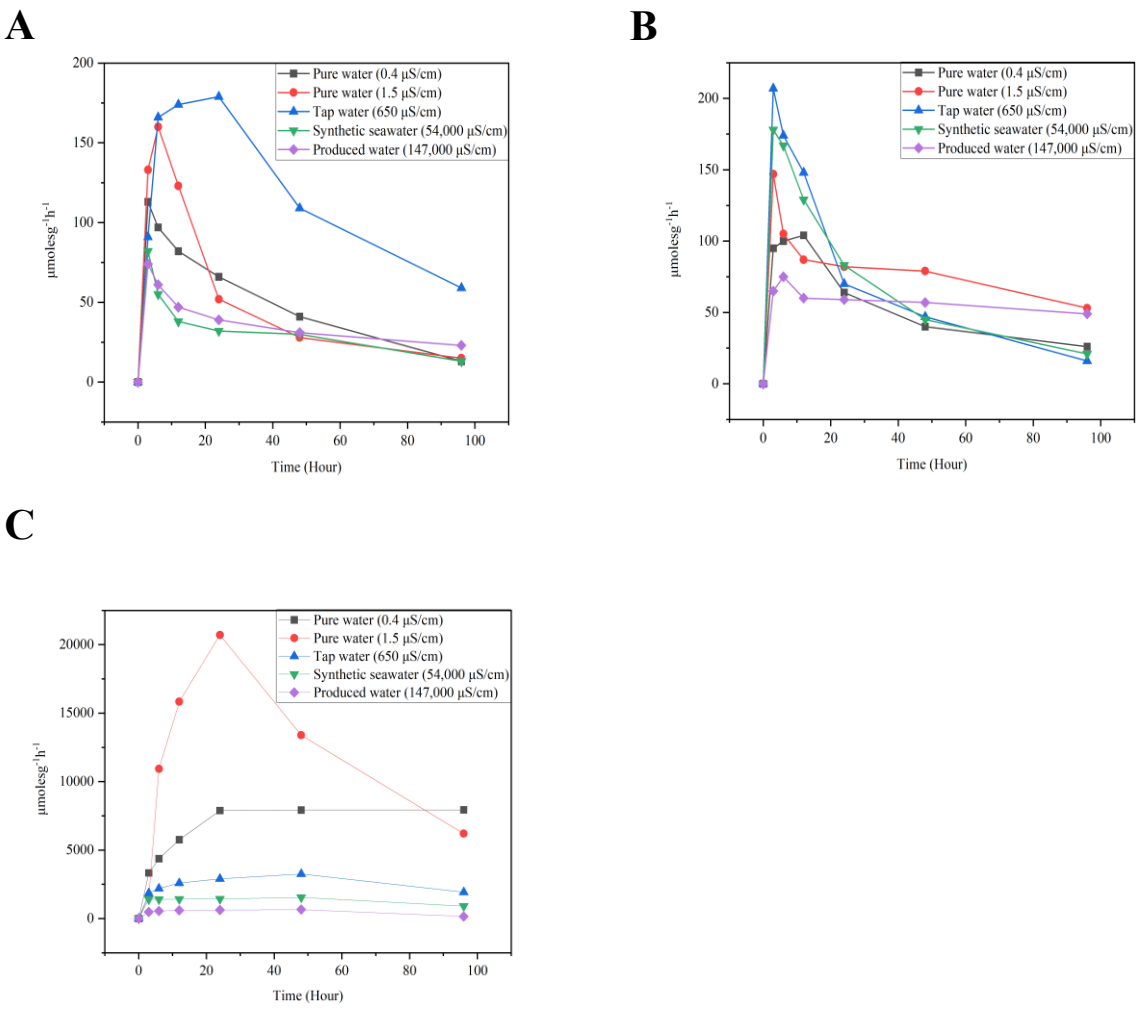


Figure 6: Hydrogen production rate using different water sources A) UV light experiment B) Visible light experiment, C) UV light experiment with sacrificial agent.

The graph analysis reveals a consistent pattern across all water types: a rapid increase in the measured parameter within the initial 3 to 6 hours of the experiment, followed by a gradual decline. Tap water exhibited the highest peak values in both light conditions, reaching 179 µmoles $g^{-1}$ $h^{-1}$ under UV light and 207 µmoles $g^{-1}$ $h^{-1}$ under visible light. Although all water types converged to relatively low values by the experiment's conclusion at 96 hours, tap water maintained the highest values throughout. The observed differences between UV and visible light experiments suggest a wavelength-dependent photocatalytic process. Visible light experiments demonstrated higher overall effectiveness, potentially due to greater light power. However, when considering hydrogen

production per unit of power input, UV light experiments showed superior efficiency. Water sample conductivity, indicative of dissolved solid content, appeared to influence photocatalytic activity. Notably, tap water exhibited high activity despite not being the purest sample. The complex compositions of tap water, synthetic seawater, and produced water likely affected photocatalytic activity, possibly due to the presence of ions or organic compounds acting as sacrificial agents, electron donors, and acceptors. Produced water yielded the lowest overall production rate, presumably due to its high salinity (TDS 98,000 mg/L). In contrast, the high activity observed with tap water, particularly under visible light, may have significant implications for practical applications of this photocatalytic system in real-world scenarios.

Comparison of UV light experiments without (Figure 6A) and with ethanol as a sacrificial agent (Figure 6C) reveals a significant enhancement in hydrogen production rates across all water sources. This effect is particularly pronounced in pure water (conductivity: 1.5 µS/cm). The introduction of a sacrificial agent, such as ethanol, inhibits the recombination of photogenerated electrons and holes, resulting in substantially increased photocatalytic activity. The more pronounced effect observed in pure water can be attributed to the reduced competition from other ions or molecules. The slight conductivity of the pure water sample may provide just enough ionic content to optimize the reaction conditions. Furthermore, the continuous presence of ethanol serves as a constant electron source, sustaining the reaction over extended periods. However, the impact of ethanol appears diminished in synthetic seawater and produced water, possibly due to their high salt content interfering with ethanol's effectiveness or the overall photocatalytic process.

The varied responses among different water types underscore the complex interactions between the photocatalyst, sacrificial agent, and water composition in determining the overall photocatalytic efficiency. These findings highlight the importance of considering water source characteristics when optimizing photocatalytic hydrogen production systems, especially when employing sacrificial agents.

## 5.5. Photocatalytic dye wastewater degradation and simultaneous hydrogen production:

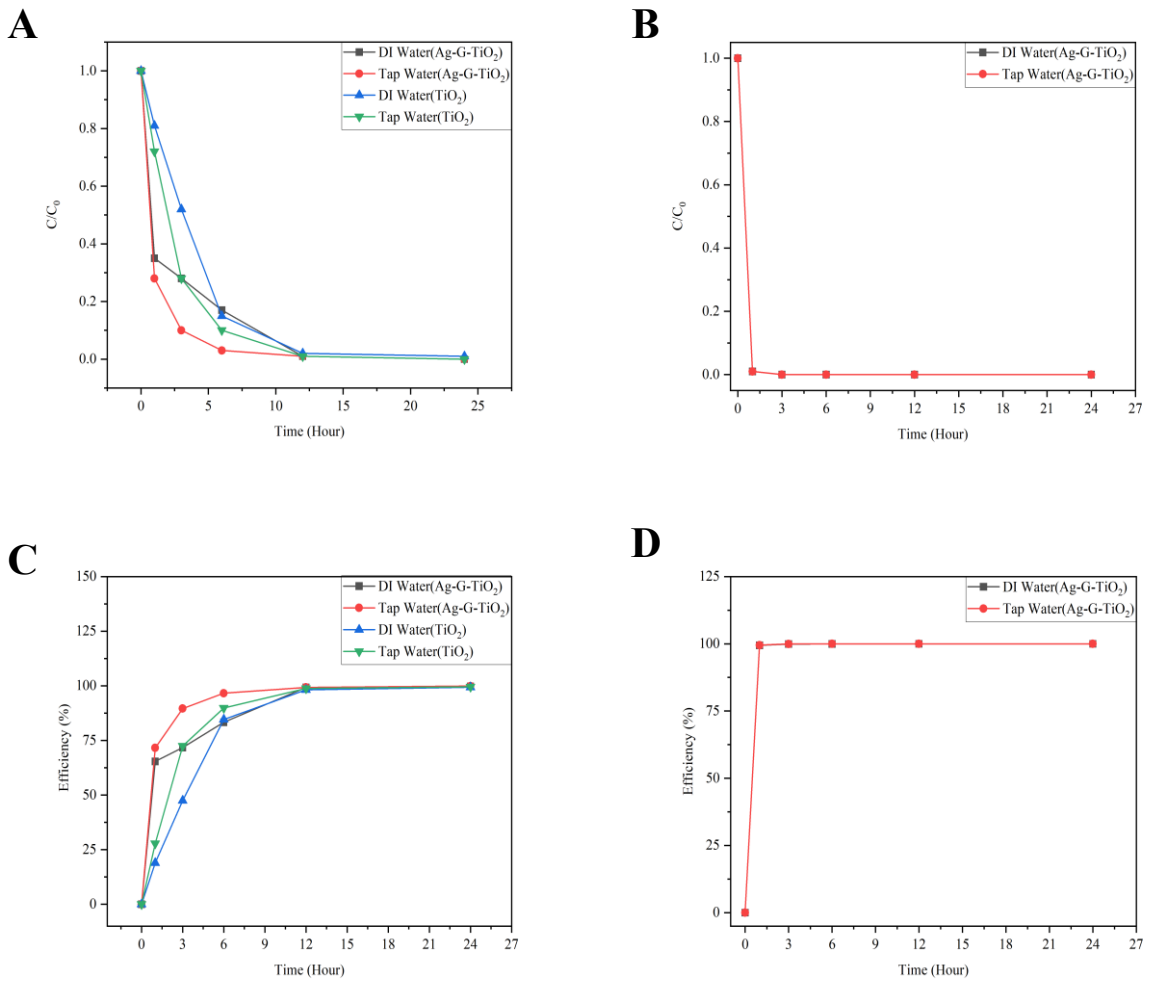


Figure 7: Photocatalytic dye waster water degradation and catalyst efficiency over time A) Visible Light, B) UV Light, C) Visible Light, D) UV Light

The visible light experiments revealed a rapid dye degradation within the first hour using the Ag-G-$TiO_2$ catalyst, indicating efficient purification. In contrast, $TiO_2$ alone exhibited significantly slower degradation under visible light. This performance disparity suggests that silver and graphene modifications enhance purification efficiency by lowering the catalyst's bandgap, enabling visible light absorption. Optimal dye degradation was achieved using Ag-G-$TiO_2$ in tap water, with dye concentration decreasing from 10 mg/L to 0.03 mg/L over 6 hours, yielding 97% efficiency. Under identical conditions with deionized (DI) water, the concentration decreased to 1.67 mg/L, corresponding to 83.3% efficiency. Similar trends were observed with pure $TiO_2$,

indicating higher performance in tap water compared to DI water. This difference may be attributed to the presence of ions or compounds in tap water acting as sacrificial agents, facilitating electron migration from the valence to the conduction band of the photocatalyst [22]. Extended experiments beyond 12 hours showed convergence to low concentration ratios across all conditions, suggesting high overall purification efficiency regardless of the specific treatment. This observation may partially be due to dye degradation by visible light itself [23].

$TiO_2$ becomes an active semiconductor under UV irradiation (< 400 nm) [24]. UV light experiments demonstrated an extremely rapid decrease in concentration ratio ($C/C_0$) for both DI and tap water solutions within the first hour. This indicates a faster and more effective purification process compared to visible light. Under UV irradiation, dye concentration decreased from 10 mg/L to 0.06 mg/L (DI) and 0.05 mg/L (tap), corresponding to efficiencies of 99.43% and 99.50%, respectively. The marked difference between visible and UV light performance can be attributed to the superior activation of Ag-G-$TiO_2$ under UV light, which more effectively generates electron-hole pairs on the catalyst surface, leading to rapid formation of reactive oxygen species for dye degradation. The performance under visible light suggests that Ag-G modification successfully extends the photocatalyst's activity into the visible spectrum, potentially through mechanisms such as plasmonic enhancement (Ag) and improved charge separation (graphene).

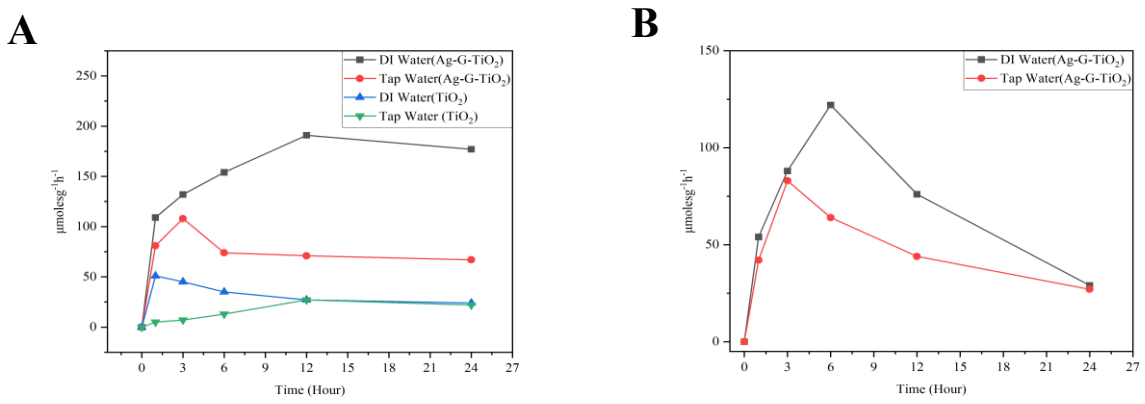


Figure 8: Photocatalytic hydrogen production A) Visible Light, B) UV Light

Photocatalytic hydrogen production experiments revealed significant differences between modified (Ag-G-$TiO_2$) and unmodified $TiO_2$ catalysts under both visible and UV light conditions. The Ag-G-$TiO_2$ catalyst demonstrated markedly superior activity, indicating the profound impact

of graphene and silver modification on catalytic performance. Under visible light irradiation, Ag-G-$TiO_2$ achieved a peak hydrogen production rate of 191 μmoles $g^{-1}$ $h^{-1}$ in deionized (DI) water dye solution, substantially higher than the 108 μmoles $g^{-1}$ $h^{-1}$ observed in tap water. This trend was consistent across both catalyst types and light sources, with DI water consistently outperforming tap water in terms of hydrogen evolution. Intriguingly, while dye degradation efficiency was superior in tap water (Figure 7(C)), hydrogen production rates were lower compared to DI water. This inverse relationship may be attributed to the presence of ions and compounds in tap water that potentially adsorb onto the catalyst surface, blocking active sites for hydrogen evolution [25]. Furthermore, these species might engage in competitive reactions, consuming some of the photogenerated electrons and reducing their availability for hydrogen production [26].

Comparative analysis of visible and UV light experiments revealed distinct kinetic profiles. UV irradiation induced a more rapid initial hydrogen production rate, whereas visible light facilitated a more sustained production, ultimately achieving the highest overall rate. Both conditions exhibited a decline in production rates after peak performance (6 hours for UV, 12 hours for visible light), potentially indicating photocorrosion of the catalyst [27,28]. The accelerated dye degradation under UV light may have contributed to catalyst degradation, resulting in lower hydrogen production rates compared to visible light conditions.

## 6. Provide a paragraph on who will benefit from your research results. Include any water agency that could use your results.

Water treatment facilities and municipalities could potentially utilize this innovative photocatalytic technology for water purification. The research demonstrates that the synthesized Ag-G-$TiO_2$ catalyst is effective in degrading organic dyes in both tap water and deionized water under visible and UV light conditions. This could be particularly valuable for treating industrial effluents or contaminated water sources. Additionally, the simultaneous production of hydrogen during the water treatment process offers an appealing dual benefit - water purification coupled with clean energy generation.

Environmental protection agencies and regulatory bodies could use these findings to inform policies on water treatment standards and renewable energy initiatives. The New Mexico Environment Department (NMED) and the U.S. Environmental Protection Agency (EPA) might

be interested in the potential of this technology for addressing water quality issues while promoting sustainable energy solutions.

Furthermore, renewable energy companies and researchers in the field of hydrogen production could benefit from the insights on photocatalytic hydrogen generation from various water sources, including tap water, synthetic seawater, and even produced water from oil and gas operations. This could be particularly relevant for organizations like the New Mexico Energy, Minerals and Natural Resources Department (EMNRD) or the U.S. Department of Energy (DOE), which are invested in advancing clean energy technologies. Lastly, the oil and gas industry in New Mexico could potentially use this technology to treat and valorize produced water, addressing both water management challenges and energy production goals simultaneously.

## 7. Describe how you have spent your grant funds. Also provide your budget balance and how you will use any remaining funds.

Please find the spent information below,

| | | |
|---|---|---|
| 890105 | BUDGET | 7,500.00 |
| 722200 | DOMESTIC TRAVEL - NON-TEAM | (300.10) |
| 732090 | SUPPLIES LAB/DEMO/EDUCATION | (417.99) |
| 752001 | PRINTING REPRODUCTION | (60.00) |
| 761700 | LAB ANALYSIS | (990.00) |
| | BALANCE AS OF 08/29/24 | 5,731.91 |

We will use any remaining funds to do High Resolution Transmission Electron Microscope (HRTEM), and Field Emission Scanning Electron Microscope (FESEM) and other analysis or measurements.

## 8. List presentations you have made related to the project.

- Strategic Water Supply: State of the Science Symposium
  - ⇒ Presentation title: Photocatalytic Hydrogen Production with Ag-G-$TiO_2$: A Green Energy Solution Using Diverse Feedstocks.
  - ⇒ Presentation type: Poster

- 20th Annual RMSAWWA/RMWEA Student Conference
  - ⇒ Presentation title: Photocatalytic Hydrogen Production with Ag-G-$TiO_2$: A Green Energy Solution Using Diverse Feedstocks.
  - ⇒ Presentation type: Poster
- 68th Annual NM Water Conference
  - ⇒ Presentation title: Photocatalytic Hydrogen Production with Ag-G-$TiO_2$: A Green Energy Solution Using Diverse Feedstocks.
  - ⇒ Presentation type: Poster

**9. List publications or reports, if any, that you are preparing. For all publications/reports and posters resulting from this award, please attribute the funding to NM WRRI and the New Mexico State Legislature by including the account number: NMWRRI-SG-FALL2023.**

- Publication: Ahasan, T., Xu, P., **Wang, H**.* (2024). Dual-Function Photocatalysis in the Visible Spectrum: Ag-G-$TiO_2$ for Simultaneous Dye Wastewater Degradation and Hydrogen Production. *Catalysts,* 14, 530.
- We anticipate publishing two more papers from the research findings.

**10. List any other students or faculty members who have assisted you with your project.**

- Dr. Pei Xu, Professor, Department of Civil Engineering, New Mexico State University.

**11. Provide special recognition awards or notable achievements as a result of the research including any publicity such as newspaper articles, or similar.**

- Received the second-place award for the poster presentation at the 20th Annual RMSAWWA/RMWEA Student Conference.

**12. Provide information on degree completion and future career plans. Funding for student grants comes from the New Mexico Legislature and legislators are**

**interested in whether recipients of these grants go on to complete academic degrees and work in a water-related field in New Mexico or elsewhere.**

I am currently pursuing my Ph.D. in Civil Engineering at New Mexico State University, with an expected completion date in May 2026. My doctoral research focuses on innovative photocatalytic technologies for water treatment and hydrogen production. Upon completion of my degree, I am highly interested in pursuing a career at a national laboratory. I believe this goal aligns with my research background and passion for advancing sustainable water and energy solutions. I also believe that working at a national laboratory would provide me with the opportunity to contribute to cutting-edge research that addresses critical environmental challenges on a national scale.

## 13. References


1. Keleş, S. E. D. A. T., & Bilgen, S. (2012). Renewable energy sources in Turkey for climate change mitigation and energy sustainability. *Renewable and Sustainable Energy Reviews*, *16*(7), 5199-5206.
2. Kaygusuz, K. (2012). Energy for sustainable development: A case of developing countries. *Renewable and Sustainable Energy Reviews*, *16*(2), 1116-1126.
3. Amin, M., Shah, H. H., Fareed, A. G., Khan, W. U., Chung, E., Zia, A., Farooqi, Zia., & Lee, C. (2022). Hydrogen production through renewable and non-renewable energy processes and their impact on climate change. *International Journal of Hydrogen Energy*.
4. Dong, Z. Y., Yang, J., Yu, L., Daiyan, R., & Amal, R. (2022). A green hydrogen credit framework for international green hydrogen trading towards a carbon neutral future. *International Journal of Hydrogen Energy*, *47*(2), 728-734.
5. Lin, L., Wang, H., & Xu, P. (2017). Immobilized TiO2-reduced graphene oxide nanocomposites on optical fibers as high performance photocatalysts for degradation of pharmaceuticals. *Chemical Engineering Journal*, *310*, 389-398.
6. Gogoi, D., Namdeo, A., Golder, A. K., & Peela, N. R. (2020). Ag-doped TiO2 photocatalysts with effective charge transfer for highly efficient hydrogen production through water splitting. *International Journal of Hydrogen Energy*, *45*(4), 2729-2744.
7. Rathi, V. H., Jeice, A. R., & Jayakumar, K. (2023). Green synthesis of Ag/CuO and Ag/TiO2 nanoparticles for enhanced photocatalytic dye degradation, antibacterial, and antifungal properties. *Applied Surface Science Advances*, *18*, 100476.

8. Jadhav, S., Kalubarme, R., Chauhan, R., Singh, A., Kale, B., Ashokkumar, M., & Gosavi, S. (2023). Nanocrystalline Ag-doped cobalt oxide as a flexible electrode material for high performance supercapacitor application. *Journal of Energy Storage*, *58*, 106326.
9. Liu, W., Chen, D., Yoo, S. H., & Cho, S. O. (2013). Hierarchical visible-light-response Ag/AgCl@ TiO2 plasmonic photocatalysts for organic dye degradation. *Nanotechnology*, *24*(40), 405706.
10. Santos, L. M., Machado, W. A., França, M. D., Borges, K. A., Paniago, R. M., Patrocinio, A. O., & Machado, A. E. (2015). Structural characterization of Ag-doped TiO 2 with enhanced photocatalytic activity. *RSC advances*, *5*(125), 103752-103759.
11. Ali, T., Ahmed, A., Alam, U., Uddin, I., Tripathi, P., & Muneer, M. (2018). Enhanced photocatalytic and antibacterial activities of Ag-doped TiO2 nanoparticles under visible light. *Materials Chemistry and Physics*, *212*, 325-335.
12. Rabhi, S., Belkacemi, H., Bououdina, M., Kerrami, A., Brahem, L. A., & Sakher, E. (2019). Effect of Ag doping of TiO2 nanoparticles on anatase-rutile phase transformation and excellent photodegradation of amlodipine besylate. *Materials Letters*, *236*, 640-643.
13. Mogal, S. I., Gandhi, V. G., Mishra, M., Tripathi, S., Shripathi, T., Joshi, P. A., & Shah, D. O. (2014). Single-step synthesis of silver-doped titanium dioxide: influence of silver on structural, textural, and photocatalytic properties. *Industrial & Engineering Chemistry Research*, *53*(14), 5749-5758.
14. Akhavan, O., Abdolahad, M., Esfandiar, A., & Mohatashamifar, M. (2010). Photodegradation of graphene oxide sheets by TiO2 nanoparticles after a photocatalytic reduction. *The Journal of Physical Chemistry C*, *114*(30), 12955-12959.
15. Ren, W., Ai, Z., Jia, F., Zhang, L., Fan, X., & Zou, Z. (2007). Low temperature preparation and visible light photocatalytic activity of mesoporous carbon-doped crystalline TiO2. *Applied Catalysis B: Environmental*, *69*(3-4), 138-144.
16. Wagner, C. D. (1990). NIST x-ray photoelectron spectroscopy (XPS) database. *(No Title)*.
17. Bharti, B., Kumar, S., Lee, H. N., & Kumar, R. (2016). Formation of oxygen vacancies and Ti3+ state in TiO2 thin film and enhanced optical properties by air plasma treatment. *Scientific reports*, *6*(1), 32355.

18. Paul, K. K., & Giri, P. K. (2017). Role of surface plasmons and hot electrons on the multi-step photocatalytic decay by defect enriched Ag@ TiO2 nanorods under visible light. *The Journal of Physical Chemistry C*, *121*(36), 20016-20030.
19. Edirisooriya, E. T., Senanayake, P. S., Wang, H. B., Talipov, M. R., Xu, P., & Wang, H. (2023). Photo-reforming and degradation of waste plastics under UV and visible light for H2 production using nanocomposite photocatalysts. *Journal of Environmental Chemical Engineering*, *11*(2), 109580.
20. Abla, F., Elsayed, Y., Abu Farha, N., Obaideen, K., Mohamed, A. A., Lee, H., ... & Kanan, S. (2023). Fabrication of high surface area tio2-moo3 nanocomposite as a photocatalyst for organic pollutants removal from water bodies. *Catalysts*, *13*(2), 362.
21. Altass, H. M., Morad, M., Khder, A. E. R. S., Mannaa, M. A., Jassas, R. S., Alsimaree, A. A., ... & Salama, R. S. (2021). Enhanced catalytic activity for CO oxidation by highly active Pd nanoparticles supported on reduced graphene oxide/copper metal organic framework. *Journal of the Taiwan Institute of Chemical Engineers*, *128*, 194-208.
22. Benz, D., Van Bui, H., Hintzen, H. T., Kreutzer, M. T., & van Ommen, J. R. (2022). Mechanistic insight into the improved photocatalytic degradation of dyes for an ultrathin coating of SiO2 on TiO2 (P25) nanoparticles. *Chemical Engineering Journal Advances*, *10*, 100288.
23. Mohammed, W., Matalkeh, M., Al Soubaihi, R. M., Elzatahry, A., & Saoud, K. M. (2023). Visible light photocatalytic degradation of methylene blue dye and pharmaceutical wastes over ternary NiO/Ag/TiO2 heterojunction. *ACS omega*, *8*(43), 40063-40077.
24. Jandaghian, F., Pirbazari, A. E., Tavakoli, O., Asasian-Kolur, N., & Sharifian, S. (2023). Comparison of the performance of Ag-deposited ZnO and TiO2 nanoparticles in levofloxacin degradation under UV/visible radiation. *Journal of Hazardous Materials Advances*, *9*, 100240.
25. Gebremariam, G. K., Jovanović, A. Z., & Pašti, I. A. (2023). The effect of electrolytes on the kinetics of the hydrogen evolution reaction. *Hydrogen*, *4*(4), 776-806.
26. Huang, Y., Wang, C., Wang, R., Zhang, Y., Li, D., Zhu, H., ... & Zhang, X. (2022). Ethanol solution plasma loads carbon dots onto 2D HNb3O8 for enhanced photocatalysis. *ACS Applied Materials & Interfaces*, *15*(1), 1157-1166.

27. Huang, K., Li, C., Zheng, Y., Wang, L., Wang, W., & Meng, X. (2022). Recent advances on silver-based photocatalysis: Photocorrosion inhibition, visible-light responsivity enhancement, and charges separation acceleration. *Separation and Purification Technology*, *283*, 120194.
28. Weng, B., Qi, M. Y., Han, C., Tang, Z. R., & Xu, Y. J. (2019). Photocorrosion inhibition of semiconductor-based photocatalysts: basic principle, current development, and future perspective. *Acs Catalysis*, *9*(5), 4642-4687.